Hindawi
Shock and Vibration
Volume 2020, Article ID 8844282, 13 pages
https://doi.org/10.1155/2020/8844282

Research Article

Sensitivity Analysis and Experimental Verification of Bolt Support Parameters Based on Orthogonal Experiment

Kun Zhang[1], **Jinpeng Su**[1,2], **Zengkai Liu**[1], **Hongyue Chen**[3], **Qiang Zhang**[1] and **Shaoan Sun**[1]

[1]*College of Mechanical and Electronic Engineering, Shandong University of Science and Technology, No. 579, Qianwangang Road, Qingdao 266590, Shandong, China*
[2]*State Key Laboratory of Mechanical System and Vibration, Shanghai Jiao Tong University, Dongchuan Road 800, Shanghai 200240, China*
[3]*School of Mechanical Engineering, Liaoning Technical University, No. 88, Yulong Road, Fuxin 123000, Liaoning, China*

Correspondence should be addressed to Jinpeng Su; suchen@alumni.sjtu.edu.cn

Received 26 March 2020; Revised 9 July 2020; Accepted 3 September 2020; Published 18 September 2020

Academic Editor: Fabio Rizzo

This paper presents a unified supporting parameter optimization procedure for the coupled bolt-rock systems by using the orthogonal experimental methods. Convergence of surrounding rock surface and deformations in the rock are taken as the objective functions for the stability of the surrounding rock of the roadway. The key support parameters of the bolt are considered as input variables. The simulation software FLAC^{3D} is employed to develop the mechanical model for the coupled bolt-rock system and the objective functions of the coupled system are therefore obtained in the software. Combining the variance and multivariate linear regression analysis, an approach is derived to investigate the sensitivity of the support parameters to the objective functions. The corresponding support parameters are then optimized. The 15106 working of a practical mine in Yangquan is taken as an example. According to the similar simulation theory, corresponding simulation experiments are performed. Thus, the proposed method is validated and its robust performance for optimization of supporting parameters of the bolt is also demonstrated. The method provides a theoretical basis for the determination of bolt support parameters for mining roadway in a fully mechanized mining face.

1. Introduction

The bolt support technology has been developed for more than a century since it was first used in the North Wales open-air shale mine in 1872 in the UK [1]. Due to its advantages such as low cost, simple operation, and less construction space, it has been widely used in surface engineering and underground chamber construction in mining tunnels, slopes, deep soil, rock foundation pits, and so forth [2–4]. In recent years, with the development of corresponding science and technology, the demand for coal resources in industry and human life is still urgent. The shallow coal resources have gradually dried up. Deep mining will therefore play more and more important roles in the coal mining engineering [5]. However, deep wells lead to more complex geological conditions in the working face and high ground stress. Hence, mining in the coal layer can severely affect the stability of the surrounding rock of the roadway and cause serious damage [6–9]. As shown in Figure 1, the bolt will fail to support the roadway. Therefore, the requirements for the surrounding rock support technology of the roadway are getting higher and higher, and it is necessary to optimize the design of the parameters of the supporting bolt, the main support equipment.

Many experts and scholars at home and abroad have conducted systematic researches on the bolt support technology. Li [10] developed a new type of bolt support device and experimentally verified the performance and reliability of the new bolt support device in three mines. Charette and Plouffe [11] proposed a bolt with constant resistance, which

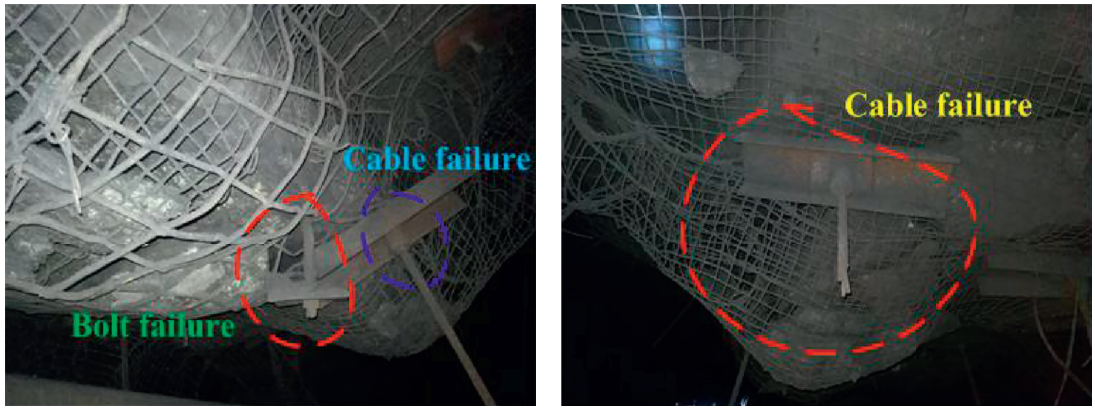

(a) (b)

Figure 1: Failure site of bolt and cable support.

is suitable for soft rock roadway support. Jager [12] designed an energy-absorbing bolt device. Varden et al. [13] put forward a new type of bolt support equipment for the geological conditions of the Kanowna Belle mine and tested its mechanical properties, using the Kalgoorlie dynamic test equipment at University of Minnesota in Australia.

Based on the elastic theory, Gu et al. [14] established a coordinated deformation model of surrounding rock and solids (rock and bolt complex) and proposed a method for evaluating the stability of the surrounding rock. Based on the asymmetrical assumption of lane strain, Wu et al. [15] established the equilibrium equation and compatibility equation of a bolt-rock system and obtained the analytical solution of the coupled model. The influences of bolt and rock properties on the transmission of the reinforcement effect in the rock were revealed. Wang et al. [16] developed a static-dynamic loading test system. The system was employed to implement the static tensile tests of equal-strength and non-equal-strength rebar bolts and the dynamic impact tests with or without prestress. Zou et al. [17] presented a strategy for excavating circular roadways in brittle and soft rocks with bolt support and established an evolution equation of the surrounding rocks with bolt support. Wang et al. [18] adopted the discrete mechanics and friction coupling (DMFC) to study the spatiotemporal evolution of the mechanical properties of the bolts and surrounding rocks. In their theoretical model, the Maxwell model was used to describe the surrounding rock, and the Kelvin model was used to describe the characteristics of the bolt. Hu and Chen [19] deduced the vibration properties of bolts subject to blasting seismic waves.

It can be found from the above literature review that coupled bolt-rock system is a sophisticated coupled mechanical system. Key parameters of the anchor bolts have significant and complex influences on the mechanical behaviors of the coupled system. Numerous example analyses will be needed if the sensitivities of all the key parameters of the bolts are equally studied. Moreover, the most useful tool to calculate the static responses of these coupled systems is numerical software such as FLAC^{3D}, which can be time-consuming. Fortunately, various orthogonal experimental methods were developed to perform the multiparameter analysis and widely used in parameter optimization for material processing, hydraulic machines, mechanical design, and so on. To date, few literatures have been published on the parameter optimization of the bolts with orthogonal experimental methods.

Motivated by this, the authors tried to develop a unified parameter optimization procedure for the coupled bolt-rock systems by using the orthogonal experimental methods. Convergence of surrounding rock surface and deformations in the rock are taken as the objective functions. The key support parameters of the bolt are considered as input variables. The simulation software FLAC^{3D} is employed to develop the mechanical model for the coupled bolt-rock system and the objective functions of the coupled system are therefore obtained in the software. Combining the variance and multivariate linear regression analysis, an approach is derived to investigate the sensitivity of the support parameters. The corresponding support parameters are then optimized. In order to validate the proposed method and to demonstrate its robust performance, a working face of a practical mine in Yangquan is taken as a numerical example and a corresponding experiment is carried out.

2. Numerical Simulation

2.1. Numerical Modeling. FLAC^{3D} is a powerful tool to calculate the stress and plastic flow of the soil and rock materials. Therefore, FLAC^{3D} is also adopted to establish the simulation model in this paper, as shown in Figure 2.

The empty part is utilized to simulate the roadway. During the excavation process, the Mohr-Coulomb constitutive model [20] is employed for the coal and rock, as shown in equation (1). The section of the roadway is formed at the same time, and the joints and faults in the rock formation are not considered. The explicit Lagrangian algorithm and hybrid-discrete partitioning technique are used for plastic failure and flow of the coal and rock in the model.

$$\sigma_1 = q_p + M_p^* \left(\frac{\sigma_3}{q_p}\right)^a, \quad (1)$$

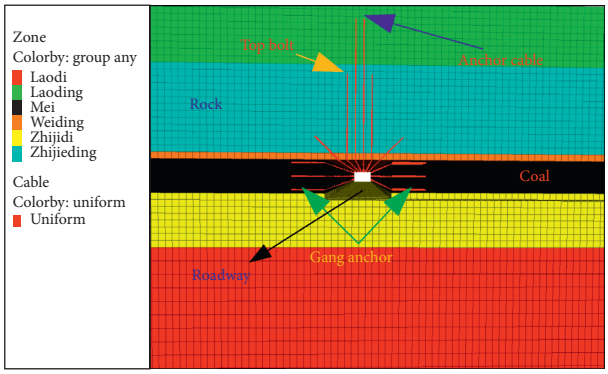

Figure 2: Experimental simulation model.

where M is the maximum principal stress; N is the minimum principal stress; M is the unconfined compressive strength of the rock measured by triaxial compression experiments.

The physical and mechanical parameters of coal and rock mass were obtained by laboratory tests. According to [21], the elastic modulus, cohesion, and tensile strength parameters of coal and rock mass during the simulation experiment were taken as 1/6 of the laboratory test results. Poisson's ratio is 1.25 times of the laboratory test results.

As for the supporting parts, the cable element is used to simulate the bolt and cables and the beam element is employed for the steel belt. The connection between the node and zone at the head of the cable is automatically established. The bolt trays are simulated with rigid chains. The free section and the bolting section of the bolts are distinguished by setting different parameters. The pretension force is applied to the free section of the bolt (cable) [20].

With regard to the boundary conditions of the model, the normal displacements of the front, back, left, and right rock surfaces in the model are restrained. The bottom of the model is fixed for displacements in all three directions.

2.2. Determination of the Compensation Load. Since the practical coal and rocks considered in this paper have infinite length, it is impossible to model the whole part of the coal and rocks in FLAC^{3D}, and the larger the mechanical model is, the more time will be consumed for the calculation. Fortunately, with proper self-weight stress added, relatively accurate results can be obtained when only a part of the rock mass is considered, and this paper is focused on the coupling between the bolt (cable) and rocks (coal). Thus, a finite length model is developed and compensation load for self-weight of the rocks unconsidered in the mechanical model is also introduced [22–24], as shown in Figure 3. H is the distance from the ground surface to the model surface in the vertical direction.

The added self-weight stress $\sigma_{z-\text{Compensation}}$ in the vertical direction may be expressed in the following equation:

$$\sigma_{z-\text{Compensation}} = \sum_{i=1}^{n} \gamma_i \times H_i, \tag{2}$$

where γ_i is the bulk density of each coal rock, $i = 1, 2, 3, \ldots$; H_i is the thickness of each coal rock layer with total length H.

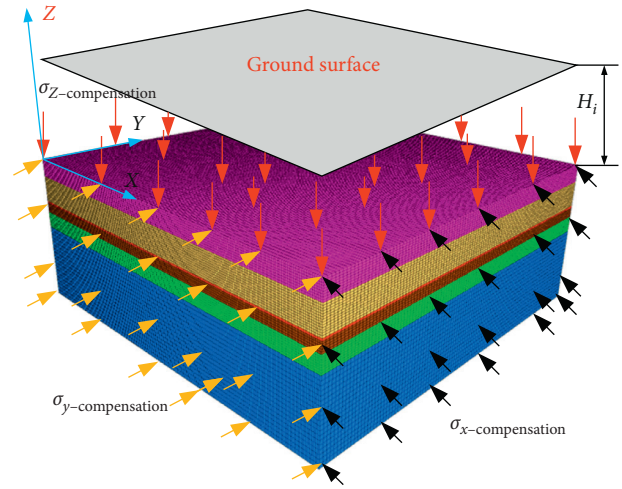

Figure 3: Schematic diagram of the experimental model's self-weight stress and compensation stress.

In the calculation, it is necessary not only to apply the self-weight stress in the vertical direction but also to compensate for the horizontal and lateral stresses σ_x and σ_y. According to the generalized Hooke's law [25, 26], the corresponding relationship between the self-weight stress in the other two directions and the vertical stress can be defined as

$$\begin{cases} \varepsilon_x = \dfrac{1}{E}\left[\sigma_x - \mu\left(\sigma_y + \sigma_z\right)\right] = 0, \\ \varepsilon_y = \dfrac{1}{E}\left[\sigma_y - \mu\left(\sigma_x + \sigma_z\right)\right] = 0, \end{cases} \tag{3}$$

namely,

$$\sigma_x = \sigma_y = \frac{\mu}{1-\mu}\sigma_{z-\text{Compensation}} = \chi\sigma_{z-\text{Compensation}}, \tag{4}$$

where χ is the side pressure coefficient of the coal rock layer.

3. Orthogonal Experiment Design and Parameter Sensitivity Analysis Method

3.1. Orthogonal Experimental Design. According to the existing research [27], 5 parameters of the bolt have considerable influences on the stability of the surrounding rock of the roadway. If the effects of the 5 parameters are tested one by one, more than 7,000 experimental schemes are required, which can be expressive. Moreover, the sensitivity of the parameters to the objective functions cannot be comprehensively studied. The orthogonal experiment provides a robust way to select some representative factors and levels from the comprehensive experiments for profound investigations [28–30]. These representative experiments have the characteristics of "uniform dispersion and neat comparison" [31], which can significantly reduce the experiment quantity, and the sensitivity of the parameters to the objective functions can also be obtained.

Therefore, the L16 (4^5) orthogonal table is employed to design the orthogonal experiment scheme. 4 levels are

selected for each parameter of the 5 support parameters of bolts, as shown in Table 1. The surrounding rock form of the roadway supported by bolts is shown in Figure 4.

According to the supporting mechanism of bolts and cables to the surrounding rock of the roadway, the convergence of the roof surface of the mining roadway and deformations in the rock (2 m away from the roadway roof) are taken as the objective functions to be optimized in the designed orthogonal experiments.

3.2. Parameter Sensitivity Analysis Method

3.2.1. Variance Analysis Method. The variance method is a mathematical method to distinguish the difference among the experimental results caused by the changes of the parameter levels and fluctuation of errors [32].

The sensitivity of the parameter to the evaluation index is judged by the sum of the squares of the total deviations S_T^2. The sum of squares of deviations caused by each parameter is expressed as S_j^2. The total sum of squared deviations and the sum of squared deviations of various factors may be expanded as

$$\begin{cases} S_T^2 = \sum_{i=1}^{n} (y_i - \overline{y}) = \sum_{i-1}^{n} y_i^2 - \frac{1}{n}\left(\sum_{i=1}^{n} y_i\right)^2, \\ S_j^2 = \frac{r}{n}\left(\sum_{i=1}^{r} y_i^2\right) - \frac{\left(\sum_{i=1}^{n} y_i\right)^2}{n}, \\ \overline{y} = \frac{1}{n}\sum_{i=1}^{n} y_i, \end{cases} \tag{5}$$

where n is the number of the experiments. r represents the number of factors. y is the assessment index value. $\overline{y}$ is the average evaluation index.

Then, the required degrees of freedom can be obtained as follows:

$$\begin{cases} f_T = n - 1, \\ f_j = r - 1, \\ f_e = \sum f_{\text{Empty column}}, \end{cases} \tag{6}$$

where f_T is the degree of freedom of the sum of squares of the total deviation. f_j is the degree of freedom of the sum of squared deviations of various factors. f_e is the degree of freedom of errors.

The analysis of variance determines the significant factors through the F test of each factor [20]. The criteria for significance of each factor are given in Table 2. The F test is calculated by

$$F_j = \frac{\left(S_j^2/f_j\right)}{\left(S_e^2/f_e\right)} F_{1-\alpha}\left(f_j, f_\Delta\right), \tag{7}$$

where S_e^2 is the sum of squares of errors; α is a significant level.

3.2.2. Multiple Linear Regression Analysis. Supposing that the objective function and the selected parameters for each experiment are y_i and x_{ij}, respectively, where $i = 1, 2, 3, \ldots, n$, $j = 1, 2, 3, \ldots, m$, and m is the number of the selected parameters, the relationship between y_i and x_i can be defined as [29]

$$y_i = \delta_0 + \delta_1 x_{i1} + \delta_2 x_{i2} + \cdots + \delta_m x_{im} + \kappa_i = \widehat{y}_i + \kappa_i, \tag{8}$$

where δ_j is the sensitivity factor of the corresponding factor. The errors κ_i are independent from each other and follow the $N(0, \sigma^2)$ distribution.

For the case with multiple objective functions y_{qi} considered in this paper and $m = 5$, equation (8) can be expanded as

$$y_{qi} = \delta_0 + \delta_1 x_{i1} + \delta_2 x_{i2} + \delta_3 x_{i3} + \delta_4 x_{i4} + \delta_5 x_{i5} + \kappa_{qi} = \widehat{y}_{qi} + \kappa_{qi}. \tag{9}$$

In order to make sure the error is the smallest, according to the principle for the extreme value [33], the sensitivity factors can be obtained by

$$\begin{cases} \widehat{\delta}_1 \sum_{i=1}^{n} (x_{i1} - \overline{x}_1) x_{i1} + \widehat{\delta}_2 \sum_{i=1}^{n} (x_{i2} - \overline{x}_2) x_{i1} + \widehat{\delta}_3 \sum_{i=1}^{n} (x_{i3} - \overline{x}_3) x_{i1} + \widehat{\delta}_4 \sum_{i=1}^{n} (x_{i4} - \overline{x}_4) x_{i1} + \widehat{\delta}_5 \sum_{i=1}^{n} (x_{i5} - \overline{x}_5) x_{i1} = \sum_{i=1}^{n} \left(y_{qi} - \widehat{y}_q\right) x_{i1}, \\ \widehat{\delta}_1 \sum_{i=1}^{n} (x_{i1} - \overline{x}_1) x_{i2} + \widehat{\delta}_2 \sum_{i=1}^{n} (x_{i2} - \overline{x}_2) x_{i2} + \widehat{\delta}_3 \sum_{i=1}^{n} (x_{i3} - \overline{x}_3) x_{i2} + \widehat{\delta}_4 \sum_{i=1}^{n} (x_{i4} - \overline{x}_4) x_{i2} + \widehat{\delta}_5 \sum_{i=1}^{n} (x_{i5} - \overline{x}_5) x_{i2} = \sum_{i=1}^{n} \left(y_{qi} - \widehat{y}_q\right) x_{i2}, \\ \widehat{\delta}_1 \sum_{i=1}^{n} (x_{i1} - \overline{x}_1) x_{i3} + \widehat{\delta}_2 \sum_{i=1}^{n} (x_{i2} - \overline{x}_2) x_{i3} + \widehat{\delta}_3 \sum_{i=1}^{n} (x_{i3} - \overline{x}_3) x_{i3} + \widehat{\delta}_4 \sum_{i=1}^{n} (x_{i4} - \overline{x}_4) x_{i3} + \widehat{\delta}_5 \sum_{i=1}^{n} (x_{i5} - \overline{x}_5) x_{i3} = \sum_{i=1}^{n} \left(y_{qi} - \widehat{y}_q\right) x_{i3}, \\ \widehat{\delta}_1 \sum_{i=1}^{n} (x_{i1} - \overline{x}_1) x_{i4} + \widehat{\delta}_2 \sum_{i=1}^{n} (x_{i2} - \overline{x}_2) x_{i4} + \widehat{\delta}_3 \sum_{i=1}^{n} (x_{i3} - \overline{x}_3) x_{i4} + \widehat{\delta}_4 \sum_{i=1}^{n} (x_{i4} - \overline{x}_4) x_{i4} + \widehat{\delta}_5 \sum_{i=1}^{n} (x_{i5} - \overline{x}_5) x_{i4} = \sum_{i=1}^{n} \left(y_{qi} - \widehat{y}_q\right) x_{i4}, \\ \widehat{\delta}_1 \sum_{i=1}^{n} (x_{i1} - \overline{x}_1) x_{i5} + \widehat{\delta}_2 \sum_{i=1}^{n} (x_{i2} - \overline{x}_2) x_{i5} + \widehat{\delta}_3 \sum_{i=1}^{n} (x_{i3} - \overline{x}_3) x_{i5} + \widehat{\delta}_4 \sum_{i=1}^{n} (x_{i4} - \overline{x}_4) x_{i5} + \widehat{\delta}_5 \sum_{i=1}^{n} (x_{i5} - \overline{x}_5) x_{i5} = \sum_{i=1}^{n} \left(y_{qi} - \widehat{y}_q\right) x_{i5}. \end{cases} \tag{10}$$

Table 1: Orthogonal experiment level design.

Influencing factors		Number of levels			
		1	2	3	4
A	Bolt spacing (mm)	700	800	900	1000
B	Bolt distance between two rows (mm)	700	800	900	1000
C	Bolt length (mm)	1800	2000	2200	2400
D	Horizontal contained angle (°)	0°	20°	40°	60°
E	Pretightening force (kN)	60	80	100	120

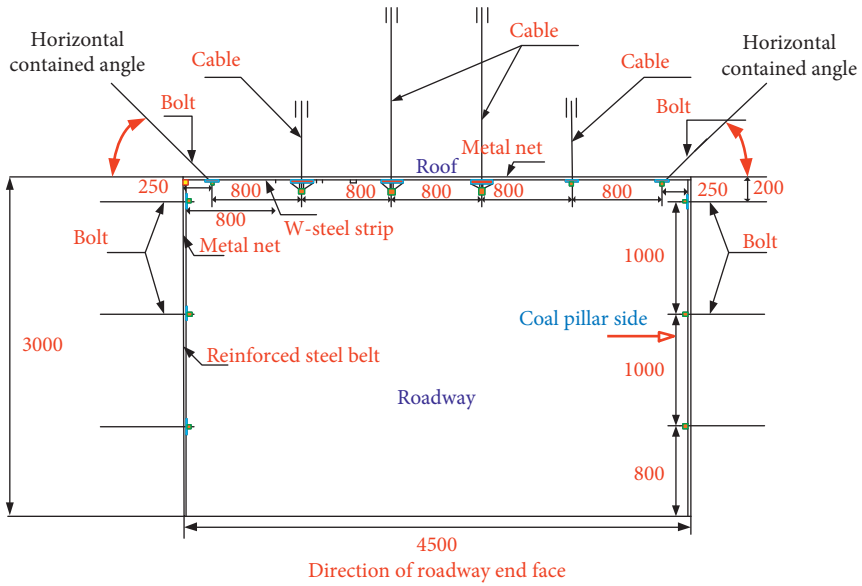

Figure 4: Working state and parameter representation of bolt.

Table 2: Significance of each factor.

F value range	Category	Sensitivity statement
$F \geq F\ 0.99$	I	Highly significant
$F\ 0.95 \leq F < F\ 0.99$	II	Generally highly significant
$F\ 0.90 \leq F < F\ 0.95$	III	Relatively remarkable
$F < F\ 0.90$	IV	Generally significant

Assume that

$$\begin{cases} g_{js} = \sum_{i=1}^{n} \left(x_{ij} - \overline{x}_j\right), \\ x_{ij} = \sum_{i=1}^{n} \left(x_{ij} - \overline{x}_j\right)\left(x_{is} - \overline{x}_s\right), \\ g_{jy} = \sum_{i=1}^{n} \left(y_{qi} - \widehat{y}_q\right), \\ x_{ij} = \sum_{i=1}^{n} \left(y_{qi} - \widehat{y}_q\right)\left(x_{ij} - \overline{x}_j\right), \end{cases} \tag{11}$$

where $j = s = 1, 2, 3, 4, 5$.

Equation (10) can be simplified as

$$\begin{cases} g_{11}\widehat{\delta}_1 + g_{12}\widehat{\delta}_2 + g_{13}\widehat{\delta}_3 + g_{14}\widehat{\delta}_4 + g_{15}\widehat{\delta}_5 = g_{1y_p}, \\ g_{21}\widehat{\delta}_1 + g_{22}\widehat{\delta}_2 + g_{23}\widehat{\delta}_3 + g_{24}\widehat{\delta}_4 + g_{25}\widehat{\delta}_5 = g_{2y_p}, \\ g_{31}\widehat{\delta}_1 + g_{32}\widehat{\delta}_2 + g_{33}\widehat{\delta}_3 + g_{34}\widehat{\delta}_4 + g_{35}\widehat{\delta}_5 = g_{3y_p}, \\ g_{41}\widehat{\delta}_1 + g_{42}\widehat{\delta}_2 + g_{43}\widehat{\delta}_3 + g_{44}\widehat{\delta}_4 + g_{45}\widehat{\delta}_5 = g_{4y_p}, \\ g_{51}\widehat{\delta}_1 + g_{52}\widehat{\delta}_2 + g_{53}\widehat{\delta}_3 + g_{54}\widehat{\delta}_4 + g_{55}\widehat{\delta}_5 = g_{5y_p}. \end{cases} \tag{12}$$

Combining equations (9) and (12), the multiple regression model can be obtained as

$$\widehat{y}_p = \widehat{\delta}_0 + \widehat{\delta}_1 x_1 + \widehat{\delta}_2 x_2 + \widehat{\delta}_3 x_3 + \widehat{\delta}_4 x_4 + \widehat{\delta}_5 x_5. \tag{13}$$

4. Analysis of Orthogonal Experiment Results

4.1. Geological Conditions. The orthogonal experimental model is based on the geological parameters of the 15106 working face of Wenjiazhuang Coal Mine in Yangquan, Shanxi Province. The experimental model shown in Figure 2 is established, and the experimental analysis is performed in conjunction with the orthogonal experimental scheme designed.

The overall shape of the 15106 working face of Wenjiazhuang Coal Mine is a monoclinic structure. The elevation of the working face is +695.3 m ~ +763.2 m, the coal seam depth is 488.3 m ~ 498.1 m, and the strike length is 1948.3 m. The air inlet roadway, air return airway, high extraction roadway, and roof low extraction roadway are dug on both sides of the working face.

The coal seam of the working face belongs to the limestone mining area under pressure in the Taiyuan Formation. Mine coal is soft, high in gas content, and poor in gas permeability. Hydrological types are classified as medium. Coal seam inclination angle is on average 6° and coal is lumpy and powdery. Mirror coal is the main, followed by bright coal, which is a bright briquette. The recoverable index of the coal seam is 1, the coefficient of variation is 9%, and the coal seam is generally stable.

The immediate roof of the No. 15 coal seam is the limestone of K2, and the thickness is 2.32 m. The main roof is sandy mudstone with a thickness of 9.05 m, including white mica flakes. The bottom is sandy mudstone with a thickness of 3.3 m, with many sandstone bands. The old bottom is fine-grained sandstone with a thickness of 4.34 m, including many black minerals and a small number of carbon shavings. The width of the roadway of the working face is 4.5 m, and the height is 3 m. The specific geological parameters for each layer are shown in Figure 5.

4.2. Analysis of Variance of Experimental Results. According to the modeling method in Section 2.1, a mechanical model for the 15106 working face is developed in FLAC^{3D}, as shown in Figure 6. The entire model size is designed to be 100 m, 100 m, and 37 m in the x, y, and z directions, respectively. The mechanical parameters of each layer of coal and rock are set according to the geological parameters in Figure 5. The average coal-rock mass Poisson's ratio is 0.3 and the average bulk density of the rock layer is 1.8 t/m^3. According to equations (2)~(4), the vertical compensation load is 717.4 t/m^3, and the compensation loads in other directions applied in the calculations are 307 t/m^3.

The convergence of surrounding rock surface and deformation in the rock of the roadway roof are monitored at 24 different positions, in which 12 monitoring points are uniformly distributed on the surrounding rock surface and 12 other monitoring points are evenly located in the rock surface, 2 m apart from the surrounding rock surface. All monitoring points are at the center-line position of the roadway roof and the distance between two adjacent monitoring points is 0.5 m, as shown in Figure 7.

Table 3 shows the variance analysis of the experimental results of the convergence of surrounding rock surface of the roadway roof with different bolt support parameters. Based on the definition of significance of a factor in Table 2, the significance of the bolt distance between two rows for the objective functions is high. The bolt preload and bolt spacing are generally highly significant, while the bolt length and horizontal angle are generally significant.

Table 4 shows the variance analysis of the experimental results for the deformations in the rock of the roadway roof with various bolt support parameters. Based on the definition of significance of a factor in Table 2, the influences of the bolt distance between two rows and the bolt preload on the deformations in the deep rock are generally highly significant. The effect of bolt length is relatively remarkable, while the effects of the horizontal angle of the bolts and bolt spacing are generally significant.

Significant impacts of the support parameters of the bolts on the convergence of surrounding rock surface and deformations in the rock of the roadway roof can be observed. In the process of supporting the surrounding rock of the roadway with bolts, bolt distance between two rows, the bolt spacing, and preload force need to be considered.

4.3. Multiple Linear Regression Analysis of Experimental Results. Using the econometric software Econometrics Views to perform multivariate linear fitting on convergence of surrounding rock surface and depth of the experimental roadway to test the established regression model to obtain the regression coefficient and reliability of the model, and then compare the regression coefficients of the model to determine the influencing factors and Correlation between evaluation indicators. Calculate the goodness of fit to determine the reliability of the regression model; the closer the goodness of fit is to 1, the higher the reliability of the regression model is. The regression coefficients and model reliability indicators of the regression model are shown in Table 5.

It can be seen from Table 5 that factor A (bolt spacing) and factor B (bolt distance between two rows) have a positive correlation with the convergence of surrounding rock surface and depth of the roadway roof. That is, the larger the bolt support row and line space, the greater the convergence of surrounding rock surface and depth of the roadway roof; and the smaller the bolt support row and line space, the smaller the convergence of surrounding rock surface and depth of the roadway roof.

Factor C (anchor length) has a negative correlation with the convergence of surrounding rock surface and depth of the roadway roof. That is, the longer the bolt rod length is, the smaller the convergence of surrounding rock surface and depth of the roadway roof. The shorter the bolt rod length, the greater the convergence of surrounding rock surface and depth of the roadway roof.

Factor D (horizontal angle of the bolt rod) has a negative correlation with the convergence of surrounding rock surface and depth of the roadway roof. The larger the horizontal angle of the bolt rod, the smaller the convergence of surrounding rock surface and depth of the roadway roof; and the smaller the horizontal angle of the bolt rod, the greater the convergence of surrounding rock surface and depth of the roadway roof.

Factor E (bolt preload) is negatively related to the convergence of surrounding rock surface and depth of the roadway roof; that is, the greater the bolt preload, the smaller the convergence of surrounding rock surface and depth of

Stratigraphic unit	Slice thickness (m)	Total thickness (m)	Columnar 1:200	Level measurement number (m)	Rock name	Lithology
Paleozoic / Carboniferous / Shangtong / Taiyuan formation	4.16	4.16			Fine-sandstone	It is mainly composed of quartz and feldspar and is jointed.
	6.28	10.44			Sandy mudstone	Brittle, flat fracture, large sand content, sandstone bands, and plant fragments fossils.
	3.22	13.66		K_4	Limestone	It is hard, the fissures are filled with cakcite veins, and the lower part is muddy.
	0.35	14.01		11	Coal seam	The coal is fast, mainly bright coal, and belongs to bright briquette.
	8.02	22.03			Sandy mudstone	Brittle, flat fracture, containing pyrite crystals, sandstone bands, and plant rhizome fossils.
	1.77	23.08		12	Coal seam	Coal is lumpy, mirror coal is the most important, and light coal is the second, 0.73 (0.30) and 0.74.
	1.09	24.89			Mudstone	It is brittle, and the fracture is uneven, rich in pyrite crystals, and fossils of plant rhizomes.
	2.46	27.35		K_3	Limestone	Hard, pure, with fine veins of calcite, marine animal fossils
	1.44	28.79			Mudstone	Brittle, flat fracture, containing pyrite crystals, calcite veins.
	0.38	29.17		13	Coal seam	Help the handle.
	4.52	33.69			Sandy mudstone	It is brittle, with uneven fractures, containing fossils of plant rhizomes, and uneven sand content.
	5.70	39.39		K_2	Limestone	Hard and pure, with fissures and fine veins of calcite.
	1.56	40.95			Sandy mudstone	Brittle, fracture-like, containing plant fossils.
	3.00	43.95			Fine-sandstone	The main ingredients are quartz and feldspar, containing a small amount of mica flakes and black minerals.
	9.05	53.00			Sandy mudstone	Brittle, flat fracture, sandstone bands, a large number of plant fragments fossils, and white mica flakes.
	2.32	55.32		K_{2under}	Limestone	Sex hard. Pure, with fine veins of calcie, cracks are not developed.
	3.16	58.48		15	Coal seam	The coal is lumpy, with bright coal as the main component, and mirror coal, followed by dark coat, which is a bright briquette. Coal seam structure is 1.16 (0.3) 1.70
	3.30	61.78			Sandy mudstone	Hard, flat fracture, large sand content, a large number of sandstone bands, containing plant rhizome fossils and pyrite crystals.
	4.34	66.12			Fine-sandstone	It is mainly composed of quartz and feldspar, containing white mica flakes, dark minerals, pyrite crystals, and is well rounded, calcareous and parallel layering.
	2.02	68.14			Sandy mudstone	Brittle, flat fracture, partly mudstone, middle and lower part containing aluminum, plant fragments fossiles, and joints.

Figure 5: Synthesis column map of 15106 working face.

the roadway roof; and the smaller the preload, the greater the convergence of surrounding rock surface and depth of the roadway roof.

Through the analysis of multiple linear regression models, the influence law of various influencing factors on the evaluation index is obtained The ranking results of the convergence of surrounding rock surface and depth of the roadway roof are consistent with the analysis results of variance, which verify the accuracy of the results of this orthogonal experiment.

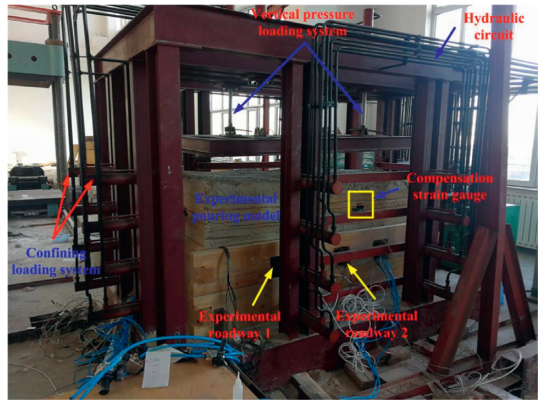

Figure 6: Frame system of the test bench and building completion model.

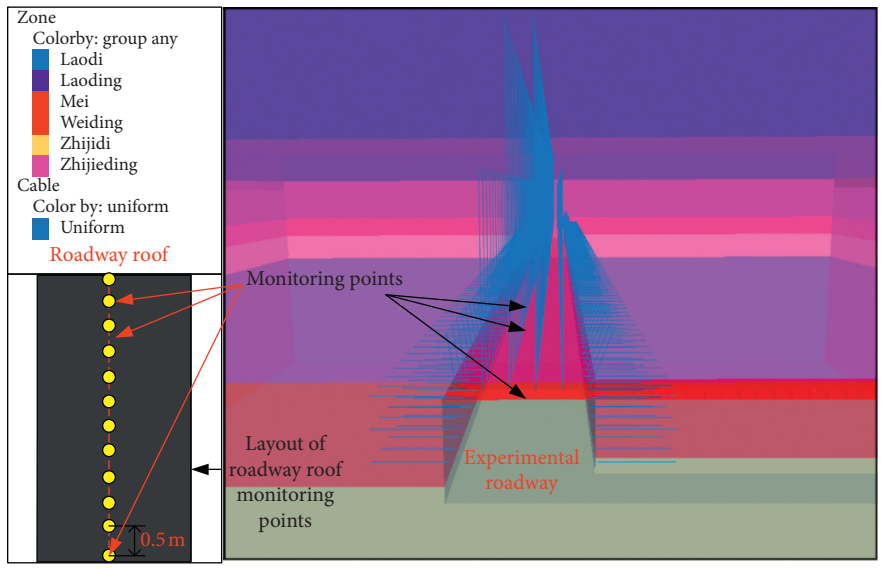

Figure 7: Orthogonal experimental model.

Table 3: Variance analysis of convergences of surrounding rock surface of the roadway roof.

Factor	Sum of squared deviations	Degrees of freedom	F value	Saliency
A	1.69	3	16.22	II
B	5.27	3	50.70	I
C	0.15	3	1.45	IV
D	0.10	3	1.00	IV
E	1.61	3	15.52	II

Table 4: Variance analysis of deformations in the deep rock (with depth of 2 m) of the roadway roof.

Factor	Sum of squared deviations	Degrees of freedom	F value	Saliency
A	0.10	3	2.89	IV
B	0.99	3	27.64	II
C	0.22	3	6.17	III
D	0.04	3	1.00	IV
E	0.35	3	9.69	II

Table 5: Regression equation coefficients and reliability tests.

Assessment index	Constant	A	B	C	D	E	Goodness of fit	Residual sum of squares
Convergence of surrounding rock surface of the roadway roof	64.23	0.004	0.005	−1.03e−4	−0.003	−0.015	0.966	0.30
Convergence of surrounding rock depth of the roadway roof	35.18	0.001	0.002	−8.24e−5	−0.022	−0.007	0.851	0.26

In the process of supporting the surrounding rock of the roadway with bolts, the smaller convergence of surrounding rock surface and depth of the roadway roof is, the more beneficial it is. Therefore, by the significance of the influence of the bolt support parameters on the convergence of surrounding rock surface and depth of the roadway roof, it can be determined that the best solution for supporting the surrounding rock of the roadway by bolts is A1B1C4D4E4 (bolt spacing 700 mm, bolt row spacing 700 mm, bolt length 2400 mm, bolt horizontal included angle 60°, and bolt preload force 60 kN).

5. Example Analysis and Similar Simulation Experiment Verification

5.1. Design of Similar Simulation Experiments. The three-dimensional similarity simulation experimental platform designed by the "Key Laboratory of Mine Subsidence Disaster Prevention of Liaoning Education Department" is employed to implement the corresponding similar simulation experiments. The test rig is shown in Figure 6.

The test system provides the equipment for the compensation loading in all the three directions. Based on the geometric size of the experimental rig, the geometric similarity constant of the similar simulation experiment is taken as 40 : 1, the bulk density similarity constant is 1.6 : 1, the time similarity constant is $\sqrt{40}$: 1, and the strength similarity constant is 64 : 1 [34, 35].

According to the synthesis column map of the coal seam 15106 in Wenjiazhuang Coal Mine, Yangquan, Shanxi, lime and gypsum as cementing materials and sand as aggregate are used for similar experimental model casting. The usage amount of the material for each layer is obtained as

$$G = l_m \times d_m \times h_m \times \gamma_m, \tag{14}$$

where G is the total weight of the model layered material. l_m is the length of the model. d_m is the model width. h_m is the thickness of the simulated layer. γ_m is the bulk density of the simulated rock formation.

Moreover, an appropriate amount of 45 mesh mica powder is added as natural bedding, and 10 mesh mica powder is used as interlayer fractures and joints. After the model is naturally dried, the surrounding baffle is removed for further drying treatment. During the drying process, an appropriate amount of watering treatment is performed every 12 hours to prevent the model from cracking due to external factors such as temperature changes. After 10 days of maintenance, the experimental test work can be carried out. Figure 6 shows the experimental model.

In order to simultaneously validate the accuracy of the mechanical model and the robust performance of the proposed method to optimize the support parameters, two cases with support parameters A1B1C4D4E4 and A2B1C2D3E4 are analyzed with both similar simulation experiments and numerical simulations. The experimental model has two experimental roadways. The No. 1 experimental roadway is used to simulate the A1B1C4D4E4 scheme support, and the No. 2 experimental roadway is used to simulate the A2B1C2D3E4 scheme support. The roadway layout is shown in Figure 8.

In the similar simulation experiment, φ19 fuse is used to simulate the bolt, and φ22 fuse is used for the anchor cable. Polyvinyl acetate emulsion is taken as the anchoring agent. A 10 mm × 10 mm × 0.5 mm iron sheet metal is employed for the bolt tray. At the same time, special pliers are used to apply the preload bolting force of the blots. To ensure the accuracy of the experiment, there is a 100 m (actual 4 m) coal pillar for the practical boundary condition at the front of the working face. As shown in Figure 9(a), there are 32 cables in 4 rows and 16 bolts in 2 rows in the roof of the roadway. A total of 6 rows of 36 simulated bolts are arranged on the left and right sides, as shown in Figure 9(c). As shown in Figure 9(a), 28 displacement sensors are employed in the experiment to measure the deformation of the roadway roof. The miniature round tube self-resetting KSP-25 mm displacement sensor, produced by Shenzhen Milang Technology Co., Ltd., is taken as the displacement sensor, as shown in Figure 9(b). The main technical parameters of the displacement sensor are shown in Table 6.

The ADAM-4117-AE (a rugged 8-way differential A/D input module) in cooperation with the acquisition programs is employed for acquisition of the displacement signals, as shown in Figure 10. The acquisition system can meet the requirements of the real-time online test and the accuracy of the test data transmission.

In the similar simulation experiment, the vertical compensation load (17.91 t/m^3) and the compensation load in the other two directions (7.7 t/m^3) are applied by using the hydraulic devices, as shown in Figure 8.

5.2. Comparison of Experimental Results. The experimental roadway after excavation is shown in Figure 11. Rock collapses and bolt fall are observed in the roof of the roadway; however, the roadway morphology remains stable.

The convergence of surrounding rock surface along the trend of the roadway at the center line of the roof in No. 1 and No. 2 experimental roadways is compared with the simulation results. Since the measured convergences of

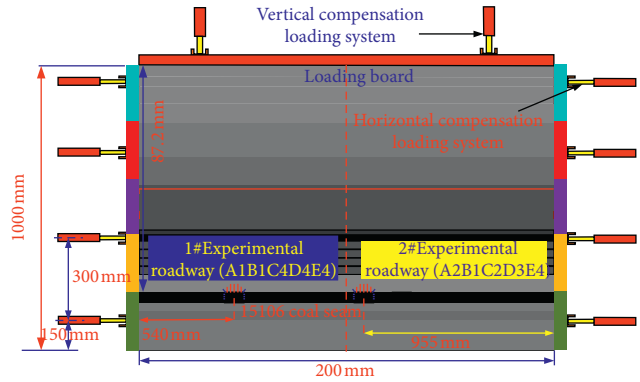

Figure 8: Similar experimental model design and experimental roadway layout.

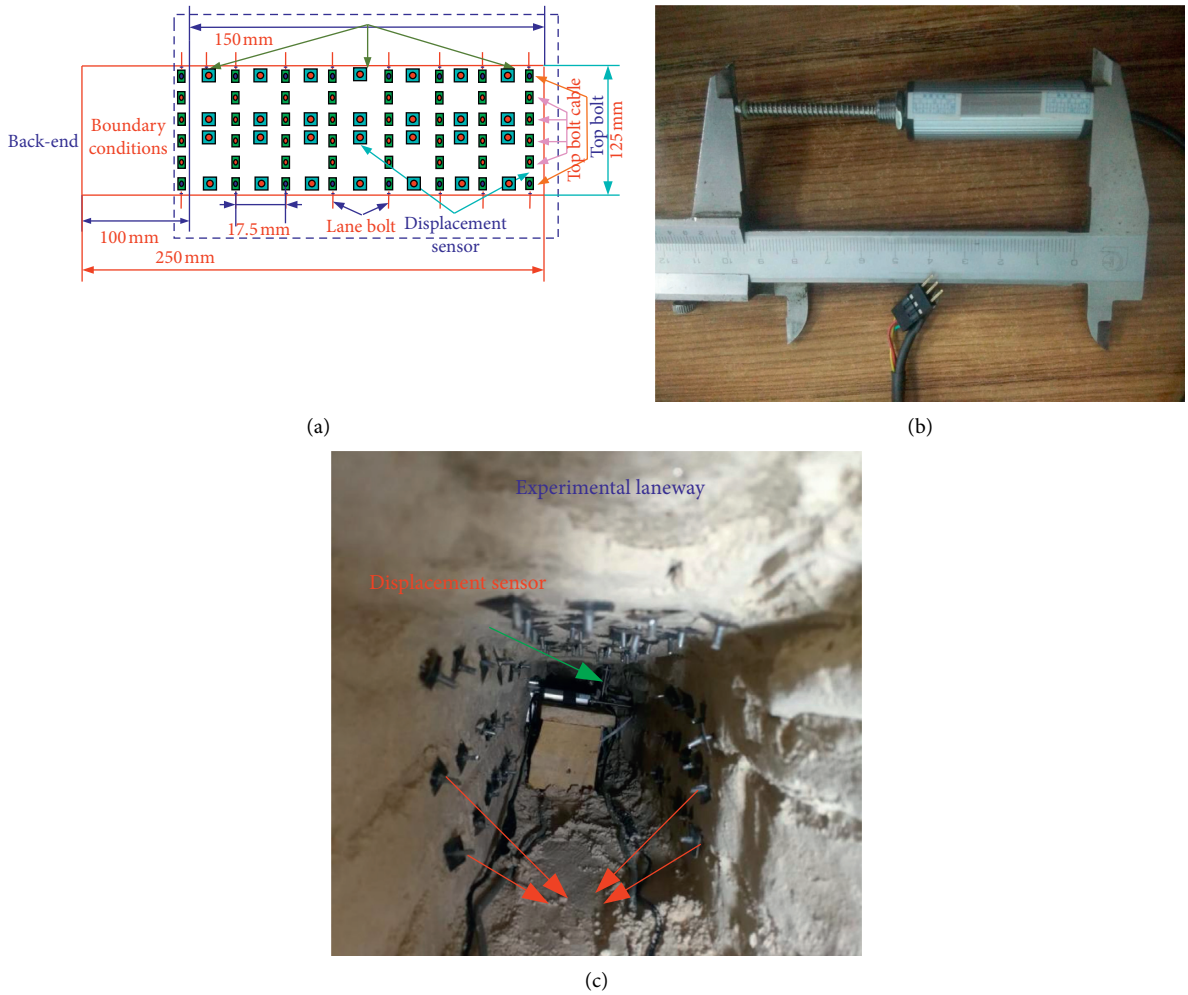

Figure 9: Simulated bolts (cables) arrangement and sensor arrangement in the experiments. (a) Simulation experiment sensor arrangement. (b) The displacement sensor. (c) Bolts (cables) layout of simulated experimental roadway.

surrounding rock surface are for the roof of roadway within 150 mm (corresponding to 6 m in practice), both numerical results and measured results for the roadway within 6 m along the roadway direction are taken for comparison and analysis. Using the geometric similarity constant and strength similarity constant, the experimental results are converted to those for the real-size model. The experimental results and numerical results are compared in Figure 12.

It can be seen from Figure 12 that the numerical results for the A2B1C2D3E4 support scheme have a maximum

Table 6: Main technical parameters of KSP-25 displacement sensor.

Linear accuracy	Sensitivity	Workload characteristic	Temperature coefficient	Repeatability errors (mm)
±0.1%	1	≥10 mA	≤1.5 ppm/°C	0.01

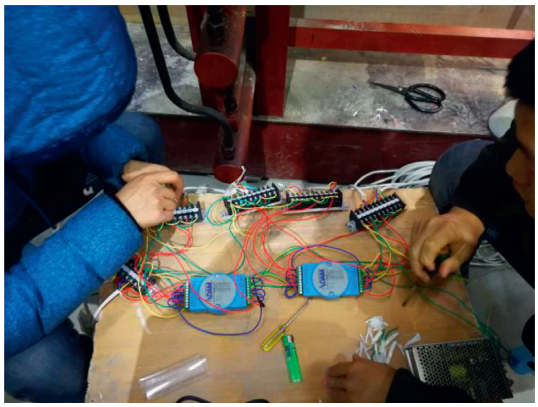

Figure 10: Experimental data test acquisition system.

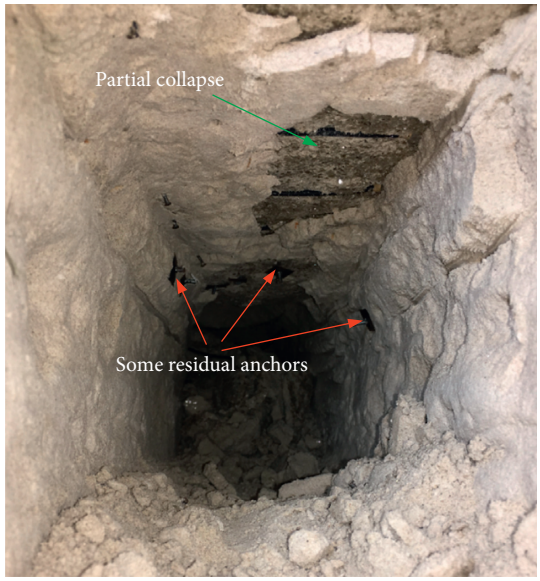

Figure 11: Roadway morphology after excavation in the experiments.

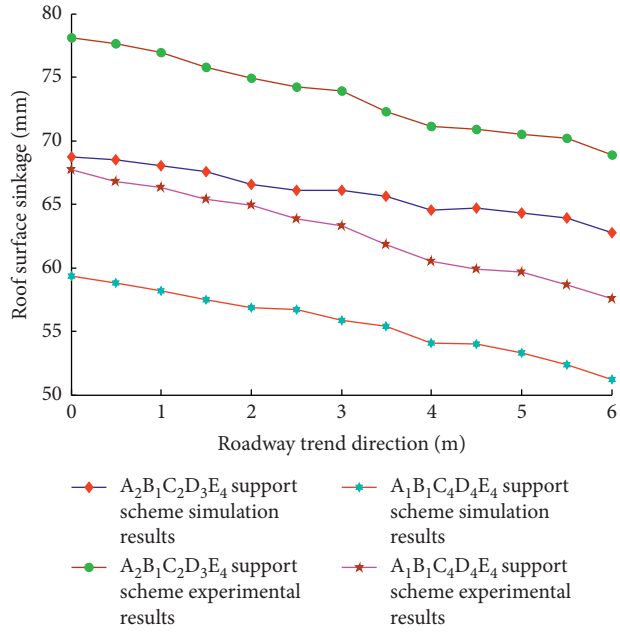

Figure 12: Comparison of experimental results and simulation results.

error of 12.06% compared with the experimental results, and the numerical results for the A1B1C4D4E4 support scheme have a maximum error of 12.33% compared with the experimental results. The distributions of the numerical results in the roadway trend directions agree well with those of the experimental results. Overall, the accuracy and reliability of the mechanical simulations in this paper are validated.

Moreover, it can be seen that the maximum convergence of surrounding rock surface at the center-line position of the roof for the A1B1C4D4E4 support scheme is reduced by 11.56 mm, compared with that for the A2B1C2D3E4 support scheme. The bolt support following the A1B1C4D4E4 support scheme can significantly decrease the convergence of surrounding rock surface and help maintain the stability of the surrounding rock of the roadway. Hence, it is demonstrated that the proposed method can be successfully employed to optimize the bolt support parameters.

6. Conclusion

This paper focuses on the sensitivity of the convergence of surrounding rock surface and deformations in the deep rock of the roadways to the bolt support parameters. Mechanical models for the rock-bolt coupled systems are developed and numerical simulations are performed in FLAC^{3D}. The orthogonal experimental method is used to design the experimental scheme, and the numerical results are analyzed by the analysis of variance. A multivariate linear regression analysis model of the bolt support parameters is established, and the influences of the key parameters of the bolts are quantified. The support parameters of the bolt are therefore optimized. Finally, corresponding simulation experiments are designed and implemented to validate the proposed mechanical model and optimal method.

It is found that the bolt spacing and the bolt distance between two rows are positively related to the stability of the surrounding rock of the roadway roof, while the anchor length, the horizontal angle of the bolt, and the bolt preload are in a negative correlation with the stability of the surrounding rock of the roadway roof. The best solution for supporting the surrounding rock of the roadway by bolts among the more than 7000 cases listed in Table 1 is the A1B1C4D4E4 support scheme. The maximum error

between the simulated results and experimental results is 12.33% and the distributions of the deformations obtained by numerical simulations and experiments agree well with each other, so that the accuracy of the mechanical model is validated. In addition, the convergence of surrounding rock surface for the optimal support scheme determined by the presented method decreases by 11.56 mm compared to that for the A2B1C2D3E4 support scheme. It is demonstrated that the proposed optimal framework provides a powerful way to optimize the support parameters of the bolt.

Data Availability

The experimental test data used to support the findings of this study are included within the article.

Conflicts of Interest

The authors declare that they have no conflicts of interest.

Acknowledgments

This work was supported by the China Postdoctoral Science Foundation (no. 2020M672089), National Key Research and Development Plan of Ministry of Science and Technology of the People's Republic of China (2017YFC0804305), and the Major Science and Technology Innovation Projects in Shandong Province (2019SDZY04).

References

[1] S. Li and Z. Wu, *Concise Course of Rock Mechanics*, Coal Industry Press, Beijing, China, 1997.

[2] L. Wang, M. Li, and X. Wang, "Study on mechanisms and technology for bolting and grouting in special soft rock roadways under high stress," *Chinese Journal of Rock Mechanics and Engineering*, vol. 24, no. 16, pp. 2890–2893, 2005.

[3] J. Bai, X. Wang, and M. Jia, "Theory and application of supporting in deep soft roadway," *Chinese Journal of Geotechnical Engineering*, vol. 30, no. 5, pp. 632–635, 2008.

[4] C. Tang, F. Chen, X. Sun, T. Ma, and Y. Du, "Numerical analysis for support mechanism of constant-resistance bolts," *Chinese Journal of Geotechnical Engineering*, vol. 40, no. 12, pp. 2281–2288, 2018.

[5] C. O. Hargrave, C. A. James, and J. C. Ralston, "Infrastructure-based localisation of automated coal mining equipment," *International Journal of Coal Science & Technology*, vol. 4, no. 3, pp. 252–261, 2017.

[6] H. Kang, J. Wang, and J. Lin, "High pretensioned stress and intensive bolting system and its application in deep roadways," *Journal of China Coal Society*, vol. 32, no. 12, pp. 1233–1238, 2007.

[7] P. Wang, H. Jia, and P. Zheng, "Sensitivity analysis of bursting liability for different coal-rock combinations based on their inhomogeneous characteristics," *Geomatics, Natural Hazards and Risk*, vol. 11, no. 1, pp. 149–159, 2020.

[8] H. Xie, F. Gao, and Y. Ju, "Research and development of rock mechanics in deep ground engineering," *Chinese Journal of Rock Mechanics and Engineering*, vol. 34, no. 11, pp. 2161–2178, 2015.

[9] W. Yu, B. Pan, F. Zhang, S. Yao, and F. Liu, "Deformation characteristics and determination of optimum supporting time of alteration rock mass in deep mine," *KSCE Journal of Civil Engineering*, vol. 23, no. 11, pp. 4921–4932, 2019.

[10] C. Li, "A new energy-absorbing bolt for rock support in high stress rock masses," *International Journal of Rock Mechanics and Mining Sciences*, vol. 47, pp. 396–404, 2010.

[11] F. Charette and M. Plouffe, "Roofex-results of laboratory testing of a new concept of yieldable tendon," *Deep Mining*, vol. 7, pp. 395–404, 2007.

[12] A. J. Jager, "Two new support units for the control of rock burst damage," in *Proceedings of the International Symposium on Rock Support*, pp. 621–631, Sudbury, Canada, June 1992.

[13] R. Varden, R. Lachenicht, J. Player et al., "Development and implementation of the garford dynamic bolt at the Kanowna Belle mine," in *Proceedings of the 10th Underground Operators' Conference*, vol. 395–404, Australian Centre for Geomechanics, Launceston, Australia, April 2008.

[14] S. Gu, P. Zhou, and R. Huang, "Stability analysis of tunnel supported by bolt-surrounding rock bearing structure," *Rock and Soil Mechanics*, vol. 39, no. 1, pp. 122–130, 2018.

[15] X. Wu, Y. Jiang, Z. Guan, and G. Wang, "Estimating the support effect of energy-absorbing rock bolts based on the mechanical work transfer ability," *International Journal of Rock Mechanics and Mining Sciences*, vol. 103, pp. 168–178, 2018.

[16] A. Wang, Q. Gao, L. Dai, Y. Pan, J. Zhang, and J. Chen, "Static and dynamic performance of rebar bolts and its adaptability under impact loading," *Journal of China Coal Society*, vol. 43, no. 11, pp. 2999–3006, 2018.

[17] J. Zou, K. Chen, and Q. Pan, "An improved numerical approach in surrounding rock incorporating rockbolt effectiveness and seepage force," *Acta Geotechnica*, vol. 13, no. 3, pp. 707–727, 2018.

[18] G. Wang, C. Liu, Y. Jiang, X. Wu, and S. Wang, "Rheological model of DMFC rockbolt and rockmass in a circular tunnel," *Rock Mechanics and Rock Engineering*, vol. 48, no. 6, pp. 2319–2357, 2015.

[19] S. Hu and S. Chen, "Analytical solution of dynamic response of rock bolt under blasting vibration," *Rock and Soil Mechanics*, vol. 40, no. 1, pp. 281–287, 2019.

[20] Z. Zhong, X. Li, Q. Yao, M. Ju, and D. Li, "Orthogonal experimental research on instability factor of roadway with coal-rock interbred roof," *Journal of China University of Mining & Technology*, vol. 44, no. 2, pp. 220–226, 2015.

[21] M. Cai, M. He, and D. Liu, *Rock Mechanics and Engineering*, pp. 69–75, Science Press, Beijing, China, 2nd edition, 2013.

[22] Q. Bai, *Mechanism and Control on Mining Induced Influences Around Longwall Top Coal Caving Face in Extra Seam with Complex Structures*, China University of Mining, Xuzhou, China, 2015.

[23] S. Yang and J. Yang, *Rock Mechanics*, Machinery Industry Press, Taichung, Taiwan, 2008.

[24] J. Li and C. Zhou, *Mine Rock Mechanics*, Metallurgical Industry Press, Beijing, China, 2016.

[25] H. Liu, *Mechanics of Materials*, Higher Education Press, Beijing, China, 2006.

[26] W. Shen, *Study on Stress Path Variation of Surrounding Rock and Mechanism of Rock burst in Coal Roadway Excavation*, China University of Mining, Xuzhou, China, 2018.

[27] L. Cai, *Study on the Stability of Wall Rock and Control Technology on Underground Mining*, Lanzhou University, Lanzhou, China, 2009.

[28] T. Yu, C. Liu, K. Yu, and W. Wang, "Experimental study on laser heat-assisted grinding quartz glass," *Journal of*

Northeastern University(Natural Science), vol. 40, no. 10, pp. 1467–1473, 2019.

[29] C. Zhou, T. Liu, H. Zhu, G. Deng, and J. Li, "Temperature prediction approach of piezo stacks used in jet valve," *Optik*, vol. 198, Article ID 163234, 2019.

[30] R. Lin, X. Diao, T. Ma, S. Tang, L. Chen, and D. Liu, "Optimized microporous layer for improving polymer exchange membrane fuel cell performance using orthogonal test design," *Applied Energy*, vol. 254, Article ID 113714, 2019.

[31] Y. Ge, Q. Liang, G. Wang, and H. Ding, *Experimental Design Method and Design-Expert Software Application*, Harbin Institute of Technology Press, 2014.

[32] W. He, W. Xue, and B. Tang, *Optimization Experiment Design Method and Data Analysis*, Chemical Industry Press, Harbin, China, 2012.

[33] G. Pastorelli, S. Cao, I. Cigić, C. Cucci, A. Elnaggar, and M. Strlič, "Development of dose-response functions for historic paper degradation using exposure to natural conditions and multivariate regression," *Polymer Degradation and Stability*, vol. 168, Article ID 108944, 2019.

[34] C. Liu, *Study on Fracture Field Evolution of Surrounding Rock and Gas Migration Law in Steeply Inclined Coal Seam with Sublevel Mining*, Xi'an University of Science and Technology, Xi'an, China, 2018.

[35] Z. Lv, *Research on Mechanism and Instability Control of Coal-Rock Mass Due to Mining Disturbance Near Fault Zone*, Xi'an University of Science and Technology, Xi'an, China, 2017.